THE JOURNAL OF PHYSICAL CHEMISTRY B

Article

pubs.acs.org/JPCB

Pretransitional Layer Contraction at the Chiral Smectic A-to-Chiral Smectic C Phase Transition of a Chiral Nitroxide Radical

Yoshiaki Uchida,*[,†] Katsuaki Suzuki,[‡] Rui Tamura,[‡] Yoshio Aoki,[§] and Hiroyuki Nohira[§]

[†]Graduate School of Engineering Science, Osaka University, 1-3 Machikaneyama-cho, Toyonaka, Osaka 560-8531, Japan

[‡]Graduate School of Human and Environmental Studies, Kyoto University, Yoshida-Nihonmatsu-cho, Sakyo-ku, Kyoto 606-8501, Japan

[§]Graduate School of Science and Engineering, Saitama University, 255 Shimo-ohkubo, Saitama, 338-8570, Japan

Supporting Information

ABSTRACT: We have designed and synthesized a new chiral paramagnetic liquid crystalline compound with a nitroxide radical moiety showing chiral smectic A (SmA*) and C (SmC*) phases. This compound shows pretransitional layer contraction prior to the SmA*-to-SmC* phase transition in the cooling run. Electron paramagnetic resonance spectroscopy, X-ray diffraction analysis, and polarized optical microscopy reveal that a temperature-dependent conformational change is responsible for the pretransitional layer contraction.

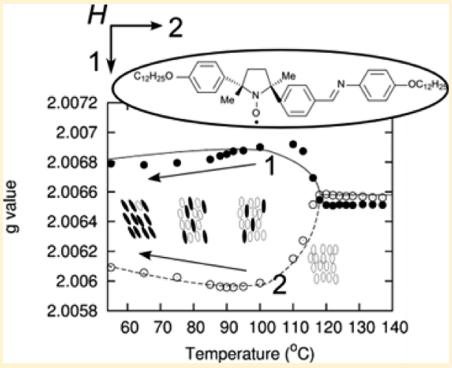

1. INTRODUCTION

Endowing liquid crystals with chirality results in the emergence of a helical superstructure and, thereby, the generation of fascinating optical and electric properties. One of these is the ferroelectricity that occurs in chiral smectic C (SmC*) phases confined in a thin sandwich cell with parallel boundary conditions.[1] Many SmC* materials, in which the director is inclined from the layer normal, exhibit a second-order transition from the untilted chiral smectic A (SmA*) phase to the SmC* phase in the cooling run. The tilting transition gives rise to a contraction of the layer spacing and thereby striking defects in the resulting SmC* phase. The formation of such defects deteriorates the quality of electro-optic devices utilizing the ferroelectric SmC* phase. On the contrary, a certain type of SmA*-to-SmC* phase transition during which the layer spacing does not change has been reported.[2,3] This unusual transition is referred to as the "de Vries type" transition.[4] In most cases, de Vries type compounds have extraordinary terminal chains such as siloxane or perfluorocarbon chains and show an extremely broad SmA*-phase temperature range.[2,5−7] It is believed that the de Vries type transition shows unusual behavior. The most famous "diffuse cone" model for this "unusual" transition was proposed by de Vries.[8] This model assumes that the SmA* molecules are not oriented along the layer normal, but rather on a cone surface around it. In this model, an ordering of the molecular azimuthal angles results in a macroscopic average tilt. Similar to SmA*-to-SmC* phase transitions, SmA-to-SmC phase transitions have been also divided into de Vries type and regular transitions.

Recently, Gorkunov et al. proposed a unified molecular statistical model to explain both the de Vries type and regular SmA-to-SmC phase transitions by using a mean-field molecular approach.[9,10] In this model, all the SmA-to-SmC phase transitions are governed by the temperature variation of the orientational order parameter S, which is identical to the second moment of the angular distribution function. The parameter S increases monotonically with decreasing temperature. When S exceeds a critical value, the SmA phase turns into the SmC phase, and tilting (θ) also occurs.

Since the SmA phase showing the regular transition generally has a high S value, there is little change in S during the SmA-to-SmC phase transition. In this case, the abrupt increase in θ leads to a large layer contraction at the phase transition. In contrast, since S in the SmA phase of de Vries type materials is exceptionally low, S grows much larger at the SmA-to-SmC phase transition. Accordingly, the rapid increase in S compensates the effect of increasing θ; this compensation leads to a constant projection of the molecular orientational distribution on the smectic layer normal at the phase transition. Korlacki et al. have confirmed experimentally that a typical de Vries-like ferroelectric liquid crystal (FLC) material exhibits IR spectra and optical properties consistent with the theory.[11]

Furthermore, Osipov et al. proposed that the pair potential of molecular directors and positions can account for the SmA*-to-

Received: January 10, 2013
Revised: February 18, 2013
Published: February 19, 2013

   dx.doi.org/10.1021/jp400325q | J. Phys. Chem. B 2013, 117, 3054−3060

SmC* phase transition; the assumption of a pair of off-center dipoles fixed in a molecular hard core enables spontaneous polarization to be explained.[12] This model is consistent with the well-established Boulder model, which can account for the ferroelectric properties of SmC* materials containing chiral dopants with two dipole moments fixed in the hard core.[13]

In this paper, we report the synthesis of an SmA*−SmC* compound (2*S*,5*S*)-**1**, which is an analogous compound of paramagnetic liquid-crystalline nitroxides **2** and **3** shown in Figure 1,[14−18] and the unusual temperature dependence of the

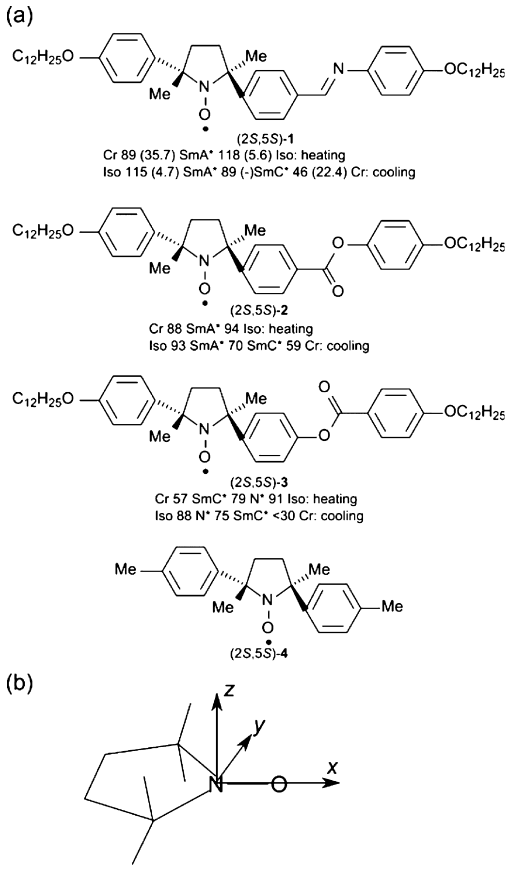

Figure 1. (a) Molecular structures and phase-transition temperatures of (2*S*,5*S*)-**1**∼**4**. The numbers in parentheses represent the Δ*H* (kJ mol^{-1}) values obtained by the DSC analysis. (b) Schematic illustration of the molecular Cartesian coordinate frame, defined as having its *x* axis along the N−O bond and its *z* axis along the p orbital on the nitrogen atom. The axes in this coordination system correspond to the principal axes of the *g*-tensor.

layer spacing of the smectic phases of (2*S*,5*S*)-**1** obtained from X-ray diffraction (XRD) analysis. This behavior is different from both regular and de Vries type transitions. To explain the behavior in terms of *S* and *θ*, we focused on electron paramagnetic resonance (EPR) spectra. The resonance magnetic field of the EPR spectrum depends on *g*-tensors, which reflects the anisotropic interactions of magnetic field with the unpaired electron fixed in the liquid crystalline molecules. We have developed a new method for fitting the temperature dependence of the *g*-value to estimate *S* and *θ* and have actually evaluated the temperature dependence of *S* and *θ* by variable-temperature EPR (VT-EPR) spectroscopy. We compare the results from XRD analysis and VT-EPR spectroscopy with the temperature dependence of *θ* obtained by the polarized optical microscopy (POM) and discuss the origin of the temperature dependence of the layer spacing in terms of the conformational distribution.

2. EXPERIMENTAL SECTION

2.1. Syntheses and Characterization. The nitroxide **5** is an intermediate for the preparation of **2**.[17,18] 4-Dodecyloxyaniline **6** was added to a solution of **5** (0.31 mmol) in benzene (20 mL), and the mixture was refluxed overnight by using a Dean−Stark trap (Scheme 1). The reaction mixture was evaporated

Scheme 1. Synthesis of (2*S*,5*S*)-1

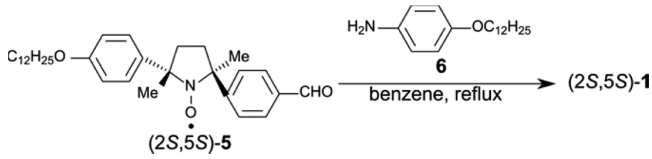

and purified by column chromatography (hexane/ethyl acetate) on silica gel to afford (2*S*,5*S*)-1-dodecyloxyphenyl-4-[(4-(4-dodecyloxyphenyl)-2,5-dimethylpyrrolidine-1-oxy-2-yl)-benzylideneamino]benzene **1** (44% yield from **5**). The ee value of **1** was determined by high-performance liquid chromatographic (HPLC) analysis using a chiral stationary-phase column (Daicel Chiralcel OD-H. 0.46 × 25 cm) (Figure S2, Supporting Information). HPLC analysis was performed using a mixture of hexane and 2-propanol (9:1) as the mobile phase at a flow rate of 1.0 mL min^{-1}, and a UV−vis spectrometer (254 nm) as the detector. The X-band EPR spectra were measured in tetrahydrofuran (THF) at 25 °C under an applied magnetic field of 0.33 T. Magnetization was recorded with QUANTUN DESIGN MPMS-2 and MPMS-5S. We measured the temperature dependence of the paramagnetic susceptibility in the temperature range 2−300 K in the first heating run. The data in the temperature range of 100−300 K were fitted to the Curie−Weiss law. The Curie constant (*C*) and Weiss constant (*θ*) were then estimated (C = 0.377 emu K mol^{-1}, θ = −0.56 K). This indicates that the nitroxide **1** is paramagnetically pure.

(2*S*,5*S*)-**1** (85% ee). Found: C, 79.60; H, 9.76; N, 3.74. Calc. for $C_{49}H_{73}N_2O_3$: C, 79.73; H, 9.97; N, 3.80%. ν_{max}(KBr)/cm^{-1} 2955, 2921, 2851, 1625, 1606, 1509, 1469, 1245, and 838. EPR: g = 2.0061, a_N = 1.33 mT (in THF). $[\alpha]^{14}_D$ −50.6° (*c* 0.086 in THF).

2.2. Measurements. The variable-temperature XRD patterns were recorded at a continuous scanning rate of 2° 2*θ* min^{-1} at a heating and cooling rate of 4 °C min^{-1} using Cu K*α* radiation (40 kV, 20 mA), with the intensity of the diffracted X-rays being collected at intervals of 0.02° 2*θ*. Differential scanning calorimetry (DSC) was performed at a scanning rate of 5 °C min^{-1}. The magnitude of P_S was determined by using 4 *μ*m cells with indium tin oxide (ITO) electrodes coated with polyimide in an electric field of 20 V peak-to-peak (5.0 V *μ*m^{-1}); P_S was measured by the triangular wave method at a frequency of 20 Hz. The optical tilt angle (*θ*) was measured as a function of the temperature between crossed Nicol polarizers under an applied electric direct-current (DC) field of 2.5 V *μ*m^{-1} and was recorded as half the rotation angle between the two extinction positions associated with oppositely directed polarization. For X-band VT-EPR spectroscopy, homeotropic boundary conditions of the cell (1.5 *μ*m thickness, 3 mm × 26 mm) were achieved by using Surfin-150 (Dainippon Ink and Chemicals, Inc.).

dx.doi.org/10.1021/jp400325q | J. Phys. Chem. B 2013, 117, 3054−3060

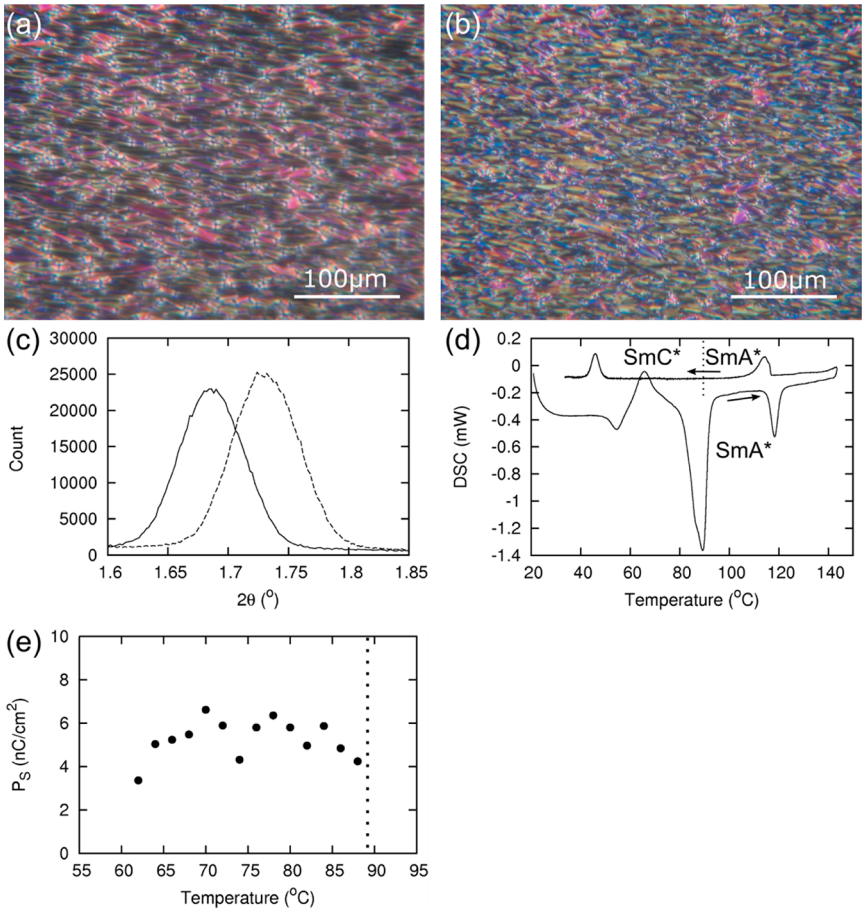

Figure 2. Optical polarized micrographs of (2*S*,5*S*)-**1** showing (a) fan-shaped texture at 100.0 °C and (b) broken fan-shaped texture at 80.0 °C in the cooling run, (c) XRD patterns of (2*S*,5*S*)-**1** at 100.0 °C (solid line, SmA* phase) and at 80.0 °C (broken line, SmC* phase) in the cooling run, (d) a DSC curve of (2*S*,5*S*)-**1**, and (e) temperature dependence of P_S of (2*S*,5*S*)-**1** in the cooling run. P_S was measured by the triangular wave method at a frequency of 20 Hz under an ac electric field of 20 V peak-to-peak (5.0 V μm^{-1}). Dotted lines represent the SmA*-to-SmC* phase-transition temperature of (2*S*,5*S*)-**1**.

3. RESULTS AND DISCUSSION

3.1. Phase-Transition Behavior. First, we characterized the phase-transition behavior of (2*S*,5*S*)-**1** by POM, DSC, and XRD analyses. (2*S*,5*S*)-**1** was confined in a glass sandwich cell with planar boundary conditions and observed by POM. (2*S*,5*S*)-**1** exhibited a liquid crystal (LC) phase in the heating run and two LC phases in the cooling run; the high-temperature LC (HLC) and low-temperature LC (LLC) phases showed fan-shaped and broken fan-shaped textures, which are typical of SmA* and SmC* phases, respectively (Figure 2a and b). A single XRD peak corresponding to the smectic layer spacing was observed for each LC phase of (2*S*,5*S*)-**1** (Figure 2c). Two endothermic peaks at 89 and 118 °C in the heating run corresponding to the crystal (Cr)-to-HLC and HLC-to-isotropic (Iso) phase transitions, respectively, were recorded in the DSC analysis, whereas two exothermic peaks at 115 and 46 °C in the cooling run were ascribed to the Iso-to-HLC and LLC-to-Cr transitions, respectively (Figure 2d). Furthermore, the spontaneous polarization (P_S) of the LC phases of (2*S*,5*S*)-**1** in a thin glass sandwich cell with parallel boundary conditions was measured, as shown in Figure 2e (see Experimental Section). P_S was detected only in the LLC phase. The P_S value gradually increased with decreasing temperature after the SmA*-to-SmC* phase transition, then started to decrease at around 70 °C, and finally could not be measured at around 60 °C (Figure 2e). These results indicate that the HLC and LLC phases correspond to enantiotropic SmA* and monotropic SmC* phases, respectively (Figure 1a). The SmA*-to-SmC* phase-transition temperature was determined on the basis of the texture change using POM and the appearance of P_S. In addition, we observed bistable switching unique to ferroelectric phases only below the SmA*-to-SmC* phase-transition temperature.

3.2. Temperature Dependence of Layer Spacing. Next, we performed variable-temperature (VT) XRD analyses in the cooling run (Figure 3). The layer spacing increased with decreasing temperature, and then the layer contraction started in the SmA* phase after reaching a peak. This behavior is different from both the regular and de Vries transitions. To explain the layer contraction in the SmA* phase by the above-mentioned uniaxial model, we developed a new method for the determination of the temperature dependence of the orientation of the nitroxide radical (NR) group by means of VT-EPR spectroscopy. In fact, for the N phase of an analogous compound **3**, the director has been confirmed to have a high correlation with the orientation direction of the NR group.[19−22]

3.3. VT-EPR Spectroscopy. The experimental setup for the VT-EPR spectroscopy is shown in Figure 4a. An LC sample was put on one side of the glass cell with homeotropic boundary conditions (see Experimental Section), which was

dx.doi.org/10.1021/jp400325q | J. Phys. Chem. B 2013, 117, 3054−3060

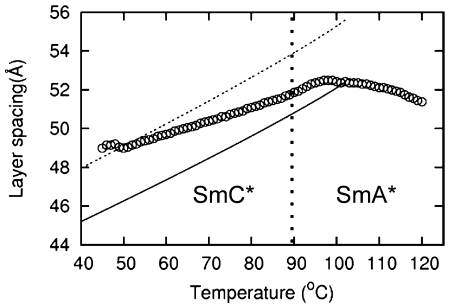

Figure 3. Temperature dependence of observed and estimated layer spacing in the SmA* and SmC* phases of (2*S*,5*S*)-**1** in the cooling run. Open circles represent the layer spacing values evaluated by XRD analysis, while the solid and broken lines show the layer spacings estimated from d_0 and l_{mo}, respectively (see text). Vertical dotted lines represent the SmA*-to-SmC* transition temperature of (2*S*,5*S*)-**1**.

located at the center of the EPR cavity in two ways; the cell plane was parallel to the magnetic field in one case (the angle (θ_0) between the smectic layer normal and the applied magnetic field for EPR spectroscopy was 90°) and perpendicular to the field in the other case (θ_0 = 0°) (Figure 4a). The former and latter cases are named configurations A and B, respectively. The EPR spectra were measured five times at the same temperature at a magnetic field of 0.33 T from 140 to 55 °C. The spectra were the Lorentzian differential curves and were fitted to the following conventional equation (eq 1)[22]

$$f(H) = -16I_m \frac{H - H_0}{\Delta H_{pp}/2} \Big/ \left\{3 + \left(\frac{H - H_0}{\Delta H_{pp}/2}\right)^2\right\}^2 \quad (1)$$

where H is the amplitude of the applied magnetic field; I_m is the maximum peak height; H_0 is the amplitude of the resonant magnetic field; and ΔH_{pp} is the peak-to-peak line width. We evaluated the g-values by referring to the peak position of the standard marker of Mn^{2+}/MgO.[19] For conformation A, the g-value started to increase at the Iso-to-SmA* phase transition and decreased with decreasing temperature after reaching a peak. In contrast, for conformation B, the g-value started to decrease at the Iso-to-SmA* phase-transition temperature and increased with decreasing temperature after reaching a minimum.

The formulation of the relationship between the g-values in configuration B (g_B) and director tilt angle (θ) is shown in the Supporting Information. When the temperature (T) is between the critical temperature for a hypothetical second-order transition from the isotropic phase to the SmA phase (T'_{IA}) and the SmA*-to-SmC* phase transition point T_{AC} in the uniaxial model (T'_{AC}), the tilt angle estimated from the EPR spectra (θ_{NR}) is 0°, and eq 2 is derived

$$g_B(T) = g_{iso} + C_0(g_{para} - g_{iso})|T - T'_{IA}|^{\gamma} + A \quad (2)$$

where g_{iso} is the g-value observed in the isotropic phase; g_{para} and g_{perp} are the g-values observed when the magnetic field is applied parallel and orthogonal to the molecular long axis, respectively; γ is a critical exponent; and C_0 and A are constants. Meanwhile, when T is smaller than T'_{AC}, θ_{NR} is not 0°. Below T'_{AC}, eq 3 is derived

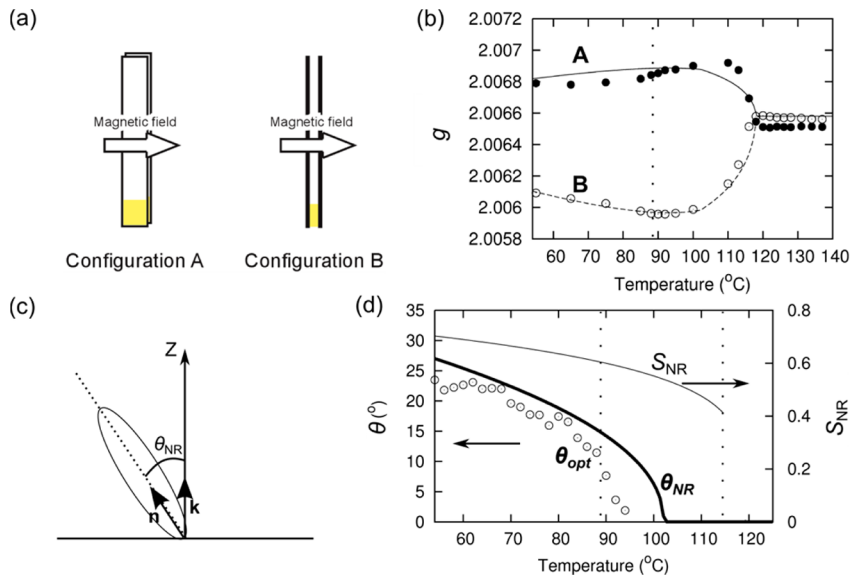

Figure 4. Evaluation of tilt angle (θ) from the temperature dependence of EPR spectra of (2*S*,5*S*)-**1**. (a) Experimental setup for VT-EPR spectroscopy. Open arrows represent the directions of applied magnetic field. The angles (θ_0) between the smectic layer normal and the applied magnetic field for configurations A and B are 90° and 0°, respectively. (b) The temperature dependence of g-values of (2*S*,5*S*)-**1** for configurations A and B are shown by symbols (●) and (○), respectively. Broken line denotes the fitted line by eqs 2 and 3 for configuration B, and the solid line shows an evaluated line for the configuration A which is based on the anisotropy of the g-tensor (eq 4). (c) A model for the orientational order parameter for the NR group (S_{NR}) at the SmA*-to-SmC* phase transition. S_{NR} is a measure of the orientational order when the orientational direction is defined as the layer normal **k**. (d) The temperature dependence of θ_{NR} estimated from EPR spectra by eqs 2 and 3 (solid line) is compared to the absolute values of the θ_{opt} (○). The temperature dependence of S_{NR} obtained by fitting the temperature dependence of g-values for the configuration B according to eqs 2 and 3 is shown as the broken line. Vertical dotted lines represent the SmA*-to-SmC* and Iso-to-SmA* phase-transition temperatures of (2*S*,5*S*)-**1**.

dx.doi.org/10.1021/jp400325q | J. Phys. Chem. B 2013, 117, 3054−3060

$$g_B(T) = g_{iso} + C_0|T - T'_{IA}|^{\gamma}\{(g_{para} - g_{iso})\cos^2(C_1|T - T'_{AC}|^{\delta}) + (g_{perp} - g_{iso})\sin^2(C_1|T - T'_{AC}|^{\delta})\} + A \quad (3)$$

where C_1 is a constant; δ is a critical exponent; and C_0 and A are the same constants as those in eq 2. Then, the temperature dependence of the g-values in configuration B could be fitted to eqs 2 and 3 as shown in Figure 4b. Some of the fitted parameters are listed in Table 1. The fitted T'_{AC} is much higher than T_{AC} observed by POM. This indicates that the molecular inclination started above the SmA*-to-SmC* phase-transition temperature. Thus, in the SmA* phase ranging from 102 to 89 °C, θ_{NR} probably occurs, and the molecular long axis is inclined from the layer normal without the ordering of the SmC director. In addition, the fitted T'_{IA} is higher than T_{IA} measured by DSC analysis. The Iso-to-SmA* phase transition is likely to be first order, as usual. The critical exponents γ and δ were evaluated as 0.196 and 0.464, respectively, which are consistent with the above-mentioned theoretical values at the Iso-to-SmA and SmA-to-SmC phase transitions.[22−25]

Table 1. Experimental and Simulated Values of Phase-Transition Temperatures and g-Values of (2*S*,5*S*)-1

	from EPR[a]	from DSC and POM	from simulation[d]
T'_{IA} (°C)	118.8	-	-
T_{IA} (°C)	-	115.0[b]	-
T'_{AC} (°C)	102.1	-	-
T_{AC} (°C)	-	89.0[c]	-
g_{iso}	2.00655	-	2.00655
g_{para}	2.00429	-	2.00467
g_{perp}	2.00768	-	2.00749

[a]These values were obtained from EPR spectra by fitting the data to eqs 2 and 3. [b]This value was obtained by DSC analysis. [c]This value was obtained by POM. [d]These values were calculated by using the experimentally evaluated principal components of the g-tensor of the nitroxide **4** and the structure of (2*S*,5*S*)-**1** obtained by molecular orbital calculations (see text).

In addition, we compared the experimentally obtained g-values in configuration A (g_A) with those estimated using the fitted parameters for the temperature dependence of g_B by eq 4,[19] as shown in Figure 4b.

$$g_A = (3g_{iso} - g_B)/2 \quad (4)$$

The fitted line exhibits the same tendency as the experimental data, though the difference between the experimental data and the fitted line is larger than that for configuration B. This result is likely to be due to the spatially nonuniform director **n**.

3.4. Molecular Orbital Calculation. To confirm that g_{iso}, g_{para}, and g_{perp} evaluated by our method are reasonable values, we calculated the g-values by conducting a coordinate transformation on a set of principal components of the g-tensor of an analogous nitroxide into the molecular long-axis frame. The molecular long axis of **1** is defined as the principal axis of inertia with the smallest inertia moment, which is calculated for the molecular structure optimized by the Monte Carlo method using the Merck Molecular Force Field, followed by AM1 semiempirical calculation using PC Spartan'02.[20] Fortunately, the EPR study of the single crystal of racemic **4** shown in Figure 1a, which has a core structure similar to **1**, gave the principal components of the g-tensor of g_x = 2.00990, g_y = 2.00639, and g_z = 2.00266, where the subscripts x, y, and z indicate the principal axes shown in Figure 1b.[21] These values have been confirmed to be valid compared with the g-tensor estimated by the classic determination in the previous paper.[19] From the principal components of the g-tensor and the simulated molecular structure, the g_{iso}, g_{para}, and g_{perp} values of **1** are calculated to be 2.00655, 2.00467, and 2.00749, respectively. These simulated g-values show the same tendency as the values obtained from the experimental data for the g-values of (2*S*,5*S*)-**1** (g_{iso} is 2.00655, g_{para} is 2.00429, and g_{perp} is 2.00768, Table 1). The simulation results clearly correspond to the experimental results, indicating that our method is effective. The unusual temperature dependence of θ_{NR} is likely to cause the pretransitional layer contraction starting in the SmA* phase.

3.5. Optical Tilt Angle. The layer spacing with a director tilt angle θ in the SmC* phase (d_C) could be represented by eq 5

$$d_C = l\cos\theta \quad (5)$$

where l is the molecular length. If l is equal to the layer spacing at T'_{AC} (d_0 = 52.48 Å) and is independent of temperature, the temperature dependence of the layer spacing can be estimated by using that of θ_{NR}, as shown in Figure 3. Whereas the estimated layer spacing is naturally equal to the spacing measured by XRD analysis at T'_{AC}, the estimated values are smaller than the experimental values in the other temperature range. This result suggests that the molecular length should grow with decreasing temperature. Meanwhile, if l is equal to the longest radius of the molecular ellipsoid calculated using the most stable molecular structure obtained from the above-mentioned molecular orbital (MO) calculation (l_{MO} = 55.61 Å), the layer spacing was estimated by substituting θ_{NR} into eq 5, shown as the broken line in Figure 3. The estimated layer spacing corresponds approximately to the spacing measured by XRD analysis at the SmC*-to-Cr phase-transition temperature, whereas the estimated values are larger than the experimental values in the other temperature range. Therefore, if the measured temperature dependence of θ_{NR} is true, the molecular length must shrink with decreasing temperature.

To examine the adequacy of the temperature dependence of θ_{NR}, we measured the optical tilt angles (θ_{opt}) under an electric field of 2.5 V μm^{-1}. The θ_{opt} values were not zero at the SmA*-to-SmC* phase-transition temperature, and the electroclinic effect was observed above the SmA*-to-SmC* phase-transition temperature (Figure 4d). θ_{opt} was close to θ_{NR} in the SmC* phase, though θ_{opt} was much smaller than θ_{NR} in the SmA* phase. These results suggest that θ_{opt} corresponds to θ_{NR} in the SmC* phase, though θ_{opt} in the SmA* phase is necessarily smaller than θ_{NR} because induced θ_{opt} is not saturated under the applied electric field. The measurement of θ_{NR} is likely to be reasonable. Furthermore, **n** should be identical to the molecular director in the SmC* phase, whereas it should not correspond to the molecular director in the SmA* phase like the molecular director in the diffuse cone model.

3.6. Molecular Conformations. When θ_{opt} was measured with further cooling, the θ_{opt} value gradually increased with decreasing temperature, and the sign of θ_{opt} turned from positive to negative at around 56 °C; the absolute value of θ_{opt} still increased with decreasing temperature (Figure 5). The sign of θ_{opt} was determined according to the reported definition.[26] We observed this odd behavior, which is referred to as "P_S sign

dx.doi.org/10.1021/jp400325q | J. Phys. Chem. B 2013, 117, 3054−3060

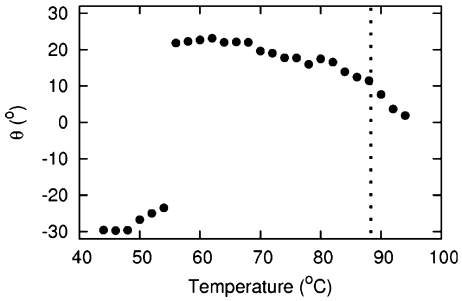

Figure 5. Temperature dependence of θ_{opt} of (2*S*,5*S*)-**1** in the cooling run. θ_{opt} was measured under an electric field of 2.5 V μm^{-1}. Dotted lines represent the SmA*-to-SmC* phase-transition temperature of (2*S*,5*S*)-**1**.

inversion" in some FLC materials.[7] Furthermore, around the P_S inversion temperature, an accurate value of θ_{opt} could not be measured because of the abrupt slowdown and stop of the ferroelectric switching to the electric field (Figure 3a).[27] The above-mentioned anomalous behavior of P_S (Figure 2e) can be attributed to the antagonistic effect between the two groups of conformational species with opposite P_S signs.

Patel et al. proposed that the presence of various competing conformational species of the molecule gives rise to the temperature-dependent P_S sign inversion.[28] In this model, two groups of conformational species are thought to have opposite P_S signs, and the relative concentrations of the two groups are assumed to be temperature dependent; then, the P_S sign inversion can be explained. The P_S inversion of **1** also can be explained in terms of Patel's model: there are two or more conformations in the SmA* and SmC* phases, and the relative concentration of molecules depends on the temperature.

Finally, we propose a hypothetical model for the origin of the pretransitional layer contraction. For the sake of simplicity, **1** is assumed to show only two conformations, *a* and *b*, with opposite P_S signs, as shown in Figure 6a; conformation *a* is the

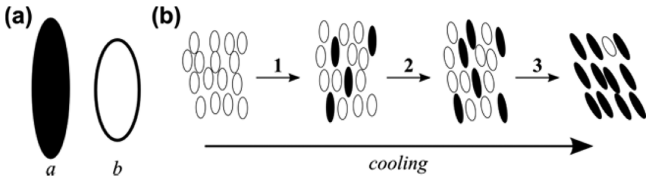

Figure 6. Schematic illustration of the relationship between the conformational distribution and the phase transition behavior. (a) Conformations *a* and *b*. (b) Conformational distribution of conformations *a* and *b* in the cooling run. 1, 2, and 3 correspond to the occurrence of θ_{NR} in the SmA* phase, the occurrence of θ_{opt} in the SmA* phase, and P_S inversion in the SmC* phase, respectively.

most stable in the SmC* phase and has a longer molecular long axis, and conformation *b* is the most stable in the SmA* phase, with a shorter molecular long axis. Conformation *a* can correspond to the most stable conformation obtained from the MO calculations. The relative concentration of these conformations of compound **1** may depend on the temperature as follows.[28] Only conformation *b* is present above T'_{AC}, and conformation *a* occurs as the temperature decreases below T'_{AC}. The NR groups in molecules with conformation *a* start tilting in the temperature range between T'_{AC} and T_{AC}; however, those in molecules with conformation *b* remain perpendicular to the smectic layers, and P_S inversion occurs when the concentration of conformation *a* exceeds a certain threshold value (Figure 6b). This is why the molecular director is averagely perpendicular to the layers, whereas **n** starts to tilt owing to the conformational change. In line with this, the conformational change could account for the pretransitional layer contraction, though the real system might be more complex. If this hypothesis were effective, the enantiomer enrichment (% ee) would affect the results. This is an open question.

4. CONCLUSIONS

We successfully synthesized a new compound showing SmA* and SmC* phases, which has a paramagnetic NR group in the core region. This compound enabled us to determine the temperature dependence of director **n** by EPR spectroscopy. The methodology for the evaluation of **n** is likely to be advantageous over the traditional technique using diamagnetic LC materials doped with paramagnetic molecules, in which a conformational distribution exists.[29] The experimental results suggest that the conformational change could play an important role in the tilting transition. The correlation between the stability of the conformation and that of the LC phases may be a universal property of the LC materials and might account for the detailed mechanism of the change in properties during the phase transitions in many cases.

■ ASSOCIATED CONTENT

Ⓢ Supporting Information

Figures S1 and S2 and additional discussion are presented. This material is available free of charge via the Internet at http://pubs.acs.org.

■ AUTHOR INFORMATION

Corresponding Author

*E-mail: yuchida@cheng.es.osaka-u.ac.jp. Tel.: +81-6-6850-6256. Fax: +81-6-6850-6256.

Notes

The authors declare no competing financial interest.

■ ACKNOWLEDGMENTS

We thank Professor Jun Yamamoto, Kyoto University, for helpful advice. This work was supported by the Grants-in-Aid for Scientific Research (No. 23245008 and 23655127) from Japan Society for the Promotion of Science (JSPS). Y.U. and K.S. are grateful to the JSPS Research Fellowships for Young Scientists.

■ REFERENCES

(1) Clark, N. A.; Lagerwall, S. T. Submicrosecond Bistable Electro-Optic Switching in Liquid Crystals. *Appl. Phys. Lett.* **1980**, *36*, 899–901.

(2) Takanishi, Y.; Ouchi, Y.; Takezoe, H.; Fukuda, A.; Mochizuki, A.; Nakatsuka, M. Spontaneous Formation of Quasi-Bookshelf Layer Structure in New Ferroelectric Liquid Crystals Derived from a Naphthalene Ring. *Jpn. J. Appl. Phys., Part 2* **1990**, *29*, L984–L986.

(3) Naciri, J.; Ruth, J.; Crawford, G.; Shashidhar, R.; Ratna, B. R. Novel Ferroelectric and Electroclinic Organosiloxane Liquid Crystals. *Chem. Mater.* **1995**, *7*, 1397–1402.

(4) Lagerwall, J. P. F.; Giesselmann, F. Current Topics in Smectic Liquid Crystal Research. *ChemPhysChem* **2006**, *7*, 20–45.

(5) Panarina, O. E.; Panarin, Yu. P.; Vij, J. K.; Spector, M. S.; Shashidhar, R. Comparison of the Characteristics of the Chiral Analog of the de Vries Type of Smectic-A* Phase. *Phys. Rev. E* **2003**, *67*, 051709-1–051709-6.

(6) Krueger, M.; Giesselmann, F. Dielectric Spectroscopy of de Vries-Type Smectic-A*−Smectic-C* Transitions. *Phys. Rev. E* **2005**, *71*, 041704−1−041704−8.
(7) Yoon, H. G.; Agra-Kooijman, D. M.; Ayub, K.; Lemieux, R. P.; Kumar, S. Direct Observation of Diffuse Cone Behavior in de Vries Smectic-A and -C Phases of Organosiloxane Mesogens. *Phys. Rev. Lett.* **2011**, *106*, 087801-1−087801-4.
(8) de Vries, A. The Implication of the Diffuse-Cone Model for Smectic A and C Phases and A−C Phase Transitions. *Mol. Cryst. Liq. Cryst. Lett.* **1979**, *49*, 179−185.
(9) Gorkunov, M. V.; Osipov, M. A.; Lagerwall, J. P. F.; Giesselmann, F. Order-Disorder Molecular Model of the Smectic-A−Smectic-C Phase Transition in Materials with Conventional and Anomalously Weak Layer Contraction. *Phys. Rev. E* **2007**, *76*, 051706-1−051706-16.
(10) Gorkunov, M. V.; Giesselmann, F.; Lagerwall, J. P. F.; Sluckin, T. J.; Osipov, M. A. Molecular Model for de Vries Type Smectic-A−Smectic-C Phase Transition in Liquid Crystals. *Phys. Rev. E* **2007**, *75*, 060701-1−060701-4.
(11) Korlacki, R.; Panov, V. P.; Fukuda, A.; Vij, J. K.; Spillmann, C. M.; Naciri, J. Orientational Order of a Ferroelectric Liquid Crystal with Small Layer Contraction. *Phys. Rev. E* **2010**, *82*, 031702-1−031702-7.
(12) Osipov, M. A.; Gorkunov, M. V.; Gleeson, H. F.; Jaradat, S. Molecular Models for Ferroelectric Liquid Crystals with Conventional and Anomalously Weak Layer Contraction. *Eur. Phys. J. E* **2008**, *26*, 395−404.
(13) Boulton, C. J.; Finden, J. G.; Yuh, E.; Sutherland, J. J.; Wand, M. D.; Wu, G.; Lemieux, R. P. Ferroelectric Liquid Crystals Induced by Dopants with Axially Chiral 2,2′-Spirobiindan-1,1′-dione Cores. *J. Am. Chem. Soc.* **2005**, *127*, 13656−13665.
(14) Ikuma, N.; Tamura, R.; Shimono, S.; Kawame, M.; Tamada, O.; Sakai, N.; Yamauchi, J.; Yamamoto, Y. Magnetic Properties of All-Organic Liquid Crystals Containig a Chiral Five-Membered Cyclic Nitroxide Unit within the Rigid Core. *Angew. Chem., Int. Ed.* **2004**, *43*, 3677−3682.
(15) Ikuma, N.; Tamura, R.; Shimono, S.; Uchida, Y.; Masaki, K.; Yamauchi, J.; Aoki, Y.; Nohira, H. Ferroelectric Properties of Paramagnetic, All-Organic, Chiral Nitroxyl Radical Liquid Crystals. *Adv. Mater.* **2006**, *18*, 477−480.
(16) Ikuma, N.; Tamura, R.; Shimono, S.; Masaki, K.; Uchida, Y.; Yamauchi, J.; Aoki, Y.; Nohira, H. Paramagnetic FLCs Containing an Organic Radical Component. *Ferroelectrics* **2006**, *343*, 119−125.
(17) Uchida, Y.; Tamura, R.; Ikuma, N.; Shimono, S.; Yamauchi, J.; Aoki, Y.; Nohira, H. Synthesis and Characterization of Novel Radical Liquid Crystals Showing Ferroelectricity. *Ferroelectrics* **2008**, *365*, 158−169.
(18) Uchida, Y.; Tamura, R.; Ikuma, N.; Shimono, S.; Yamauchi, J.; Aoki, Y.; Nohira, H. Synthesis and Characterization of Novel All-Organic Liquid Crystalline Radicals. *Mol. Cryst. Liq. Cryst.* **2007**, *479*, 213−221.
(19) Griffith, O. H.; Cornell, D. W.; McConnell, H. M. Nitrogen Hyperfine Tensor and g Tensor of Nitroxide Radicals. *J. Chem. Phys.* **1965**, *43*, 2909−2901. Noda, Y.; Shimono, S.; Baba, M.; Yamauchi, J.; Ikuma, N.; Tamura, R. EPR Studies on Molecular Orientation in a Surface-Stabilized Paramagnetic Liquid Crystal Cell. *J. Phys. Chem. B* **2006**, *110*, 23683−23687.
(20) Uchida, Y.; Tamura, R.; Ikuma, N.; Shimono, S.; Yamauchi, J.; Shimbo, Y.; Takezoe, H.; Aoki, Y.; Nohira, H. Magnetic-Field-Induced Molecular Alignment in an Achiral Liquid Crystal Spin-Labeled by a Nitroxyl Group in the Mesogen Core. *J. Mater. Chem.* **2009**, *19*, 415−418.
(21) Noda, Y.; Shimono, S.; Baba, M.; Yamauchi, J.; Uchida, Y.; Ikuma, N.; Tamura, R. EPR Study of Single Crystals of PROXYLs. *Appl. Magn. Reson.* **2008**, *33*, 85−93.
(22) Haller, I. Thermodynamic and Static Properties of Liquid Crystals. *Prog. Solid State Chem.* **1975**, *10*, 103−118.
(23) Manjuladevi, V.; Madhusadana, N. V. High Pressure Studies on a Nematogen with Highly Polar Molecules: Evidence for a Nematic−Nematic Transition. *Curr. Sci.* **2003**, *85*, 1056−1061.
(24) Yildiz, S.; Ozbek, H.; Glorieux, C.; Thoen, J. Critical Behaviour at the Isotropic−Nematic and Nematic−Smectic A Phase Transitions of 4-Butyloxyphenyl 4′-Decyloxybenzoate Liquid Crystal from Refractive Index Data. *Liq. Cryst.* **2007**, *34*, 611−620.
(25) de Gennes, P. G.; Prost, J. *The Physics of Liquid Crystals*; Oxford University Press: New York, 1993.
(26) Mieda, Y.; Hoshi, H.; Takanishi, Y.; Takezoe, H.; Zeks, B. Mechanism of Sign Inversion of Spontaneous Polarization in Ferroelectric SmC* Liquid Crystals. *Phys. Rev. E* **2003**, *67*, 021701.
(27) Mikami, N.; Higuchi, R.; Sakurai, T.; Ozaki, M.; Yoshino, K. Anomalous Dielectric Behaviour in Biphenyl Ester Series of Ferroelectric Liquid Crystals. *Jpn. J. Appl. Phys.* **1986**, *25*, L833−L835.
(28) Patel, J. S.; Goodby, J. W. Observation of Polarization Sign Inversion in Ferroelectric Liquid Crystals Produced by Doping Sc Liquid Crystals. *J. Phys. Chem.* **1987**, *91*, 5838−5840.
(29) Nayeem, A.; Rananavare, S. B.; Sastry, V. S. S.; Freed, J. H. Heisenberg Spin Exchange and Molecular Diffusion in Liquid Crystals. *J. Chem. Phys.* **1989**, *91*, 6887−6905.